Journal of Hydroscience and Hydraulic Engineering
Vol. 4, No. 1, April, 1986, pp.31-50.

ANALYSIS ON SELECTIVE WITHDRAWAL FROM THREE-LAYERED STRATIFIED SYSTEMS AND ITS PRACTICAL APPLICATION

By

Akira MUROTA

Professor, Department of Civil Engineering
Osaka University, Suita City, Osaka 565, Japan

and

Kohji MICHIOKU

Research Associate, Department of Civil Engineering
Osaka University, Suita City, Osaka 565, Japan

SYNOPSIS

A density stratification with two distinct pycnoclines is generally produced in large reservoirs by the combined actions of surface heat exchange and substantial through-flows, or by the inflowing of suspended materials into the reservoir. An experimental and theoretical investigation for a three-layer system having two distinct interfaces is undertaken here to gain insight into the characteristics of withdrawal flow fields in such practical systems. First, the flow pattern and withdrawal characteristics in a two-layer system are examined. Second, extending the work on the two-layer system to the case of three-layer one, we devise an analytical method for evaluating the withdrawal ratio in each layer. The proposed analysis is also applied to two examples of practical problems in real reservoirs. One of them is the effective removal of turbid middle layer from a reservoir. Another application of this study concerns the introduction of the present analysis to our numerical model for the prediction of thermal fields in a reservoir. From these results, we find the present work to be highly useful in engineering aspects.

INTRODUCTION

The problem of selective withdrawal from stratified density fields is one of practical importance. This problem is encountered in various engineering aspects, such as condensor water intakes for industrial cooling-water systems from coastal waters, irrigation water intakes, removal of turbid water from stratified reservoirs, and similar applications.

In most experimental and theoretical models on the selective withdrawal, the ambient density stratification is represented as a two-layer system with a distinct interface, or a continuously stratified system with a constant density gradient (2). Neither of these models, however, can precisely describe the water mass behavior when two pycnoclines with steep local density gradients are formed due to the combination of surface stirring and substantial through-flows in a reservoir. Fig. 1 shows a typical example of such temperature fields observed in a pumped storage reservoir. From May to September there exist two distinct thermoclines, one near the water surface and the other in the lower regions. Due to the stirring effect of successive pumping operation, a vertically uniform distribution of temperature develops inside the intermediate layer between the two thermoclines. After flood inflow transporting fine sediment or dissolved materials into some intermediate level of neutral buoyancy in the reservoir, the internal density fields also exhibit a typical three-layer structure, as shown in Fig. 2 (1). Two

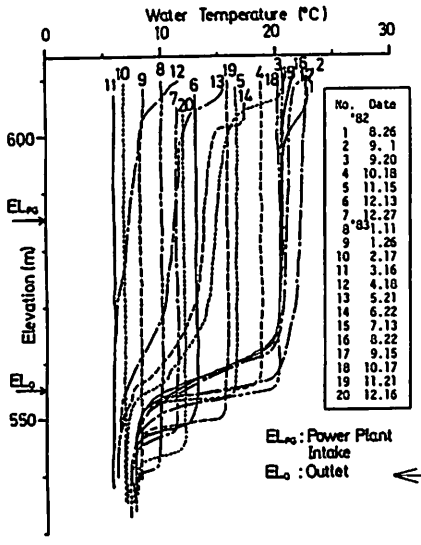

Fig. 1 Vertical profiles of observed water temperature in a pumped storage reservoir

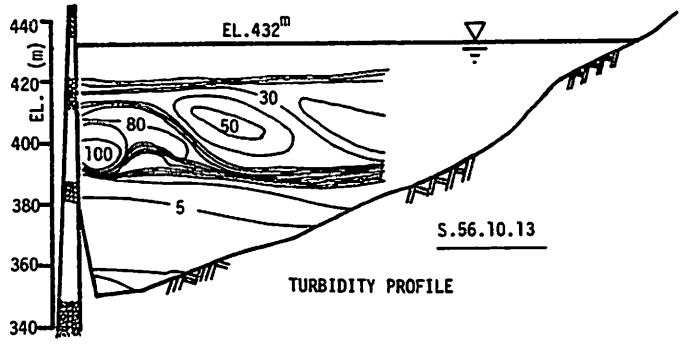

Fig. 2 Formation of turbid middle-layer after flood inflow (After Agemori(1))

distinct density interfaces composed of heat and turbidity concentration are found in this case. Between them a turbid middle layer is developed. Most of the foregoing reservoir models adopt the theory of the linearly stratified system to analyze withdrawal flow fields, even in such discretely stratified systems. These models can reproduce the thermal fields with good accuracy neverthless they neglect the local buoyancy effects within the thermocline. However, it seems unreasonable that a several empirical parameters, e.g., depth and width of the flowing layer, equivalent value of constant density gradient, eddy viscosity, critical densimetric Froude number, etc., is introduced in such models so as to fit the prediction to the observed data. Therefore, understanding the withdrawal characteristics of the three-layer system is of practical importance, both in the modeling of water mass behavior and in water quality management in reservoirs. Intending to gain insight into dynamics of the withdrawal flow in such a system, the authors will carry out fundamental laboratory experiments and devise a theory to evaluate the discharge from each layer. The proposed theory is compared with experimental results.

The present work is also applied to the following two real reservoir problems.

(a) Removal of turbid middle-layer water from stratified reservoirs

Since prolonged retension of some particulate matters in the reservoir often results in crucial troubles in the hydrospheric environment, it is strongly desired that turbid water must be removed as soon as possible. Based on our theory, we show the optimum outlet level to selectively withdraw only the middle-layer fluid from the three-layer system. According to our method, we can operate the selective withdrawal equipments in the most effective way to remove the turbid water in the middle layer from a reservoir.

(b) Prediction of thermal fields in reservoirs

A numerical model for the prediction of thermal stratification in a reservoir is devised by extending the proposed analysis to a three-dimensional system. The present analysis well describes the flow fields containing advective heat transport in a reservoir. The predicted thermal structure well explains the annual cycles of thermal fields observed in practical sites.

EXPERIMENTAL EQUIPMENT AND PROCEDURE

The experiments are carried out in the lucid plastic-walled tank shown in Fig. 3. The tank is 9.0m long, 0.3m wide and 1.0m maximum depth with a bottom slope of 1/10. A 2.0-meter-long vertical partition (1. in the figure) and a bottom plate (2. or 2'. in the figure) are placed in order to obtain a uniform two-dimensional flume of 0.1m wide and 2.0m long. This way makes possible to reduce the total quantity of discharge and minimize the effects of the associated decrease in

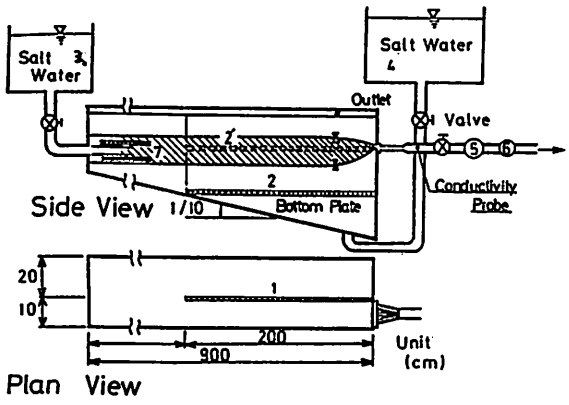

Fig. 3 Experimental equipment

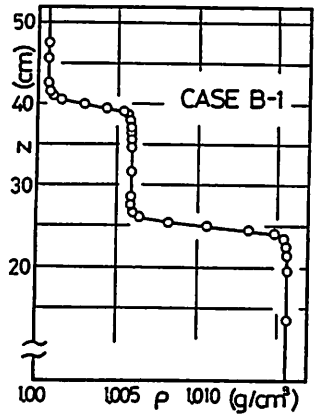

Fig. 4 Initial profile of salinity concentration

depth. A two-dimensional slot at the downstream vertical end of the tank consists of a square section 10cm wide and 0.5cm high. This slot is connected to the manifold hoses leading to the suction pump. Density stratification is produced by filling the tank with one layer of fresh water and two layers of salt water, of different concentrations, to determined layer depths. Fig. 4 represents an example of density profiles measured with the conductivity probe, which shows that a typical three-layered stratification with two distinct interfaces is formed. In order to determine the flow rate from each layer by measuring the fluorescence intensity of outflow, the middle layer is colored with fluorescent dye. Intake flow-rates are measured with a float-type flow meter, downstream from the sink. Flow velocity is measured by the hydrogen bubble method and metheylene blue dye as well. Throughout the experiment, the salinity concentration and fluorescence intensity of outflow are monitored by the conductivity probe and the fluoro photometer, respectively, placed just downstream of the outlet. The flow discharge from each layer can be simply determined from the records of salinity concentration and fluorescence intensity of outflow water, C_o and f_o. From the conservation of volume and concentration, each layer discharge is related to C_o and f_o as:

$$q_A=\{(C_o-f_o/f_B\cdot C_B)/C_C-f_o/f_B\}q_t \quad (1)$$

$$q_B=f_o/f_B\cdot q_t \quad (2)$$

$$q_C=(C_o-f_o/f_B\cdot C_B)C_o\cdot q_t \quad (3)$$

where q_A, q_B, q_C = discharges per unit width from the upper, middle and lower layers, respectively; $q_t(=q_A+q_B+q_C)$ = total intake flow rate per unit width; C_o, f_o = observed salinity concentration and fluorescence intensity of the outflow water, respectively; f_B = predetermined fluorescence intensity of the middle-layer fluid, and C_B, C_C = salinity concentration of the middle- and lower- layer fluids, respectively.

The following two series of experiments are carried out.

(a) EXPERIMENT I ; Two-layer system with the point sink at the bottom corner (Fig. 5(a)).

(b) EXPERIMENT II ; Three-layer system with the point sink located at the middle portion of the vertical boundary (Fig. 5(b)).

The system in EX. I has an analogous geometry to the upper and lower subsystems in EX. II, subdivided by the horizontal plane through the sink. EX. I is carried out to obtain fundamental information on the flow fields and withdrawal characteristics. The obtained data are then applied to the analysis of the three-layer system. Experimental conditions in each series are listed in Tables 1 and 2, respectively.

Table 1 Experimental conditions (EXPERIMENT-I)

CASE	h_1 (cm)	h_2 (cm)	$\varepsilon \times 10^{-3}$	Fr
A-1	5.0	5.0	4.7	0.393~1.31
A-2	7.0	8.0	5.1	0.427~1.36
A-3	9.0	10.0	1.0	0.552~1.86
A-4	5.0	10.0	1.0	0.584~1.39
A-5	5.0	6.0	9.9	0.543~1.30
A-6	10.0	5.0	9.9	0.487~2.11
A-7	10.0	10.0	1.3	0.246~1.34
A-8	10.0	10.0	5.3	0.224~1.26

Table 2 Experimental conditions (EXPERIMENT-II)

CASE	$\varepsilon_1 \times 10^{-3}$	$\varepsilon_2 \times 10^{-3}$	d_1 (cm)	d_2 (cm)	q_i (cm^3/s)
B-1	5.05	9.79	9.0	5.0	16.7~50.7
B-2	4.95	4.87	9.0	5.0	16.7~50.0
B-3	3.10	9.81	7.0	7.0	13.3~75.0
B-4	5.00	1.89	6.0	12.0	16.7~66.7
B-5	2.85	10.2	9.0	5.0	16.7~50.0
B-6	9.74	1.09	5.0	10.0	13.3~38.3
B-7	10.1	4.70	3.0	6.0	3.8~46.7

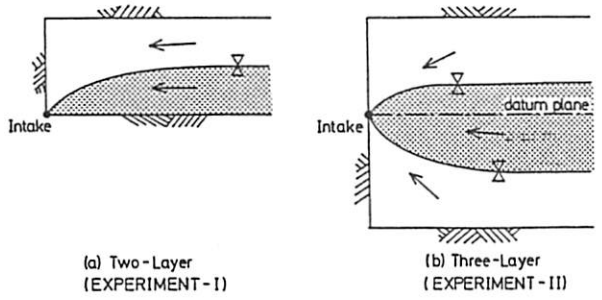

Fig. 5 Schematic of experimental systems

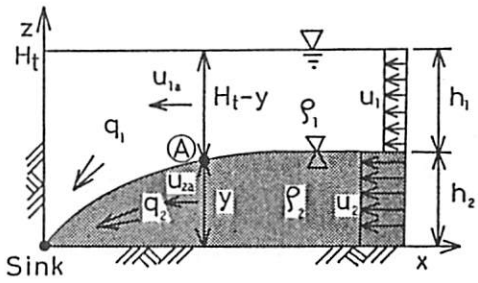

Fig. 6 Schematic of a two-layer system

WITHDRAWAL FROM A TWO-LAYER SYSTEM

Theory

As the first step of the present work, we consider a two-layer system with the point sink at the bottom corner, as shown in Fig. 5(a). This system geometrically corresponds to the upper or lower subdivision in the three-layer system shown in Fig. 5(b), divided by the horizontal datum plane through the sink. The primary purpose of the following analysis in this section is to obtain fundamental information on the flow pattern, the critical condition for the incipient drawdown of interface, and a withdrawal ratio between two layers to be applied to the three-layer case.

The flow configuration under the study is schematically shown in Fig. 6. The viscosity effect is assumed negligible and the flow irrotational as well as two-dimensional. A point sink is located at the bottom corner of the rectangular container in which two fluid strata of different densities extend to infinity in the horizontal direction.

We assume that the flow has quasi-uniform velocity distributions in each layer, and that the streamline curvature effects are negligible at the control section A where the square sum of densimetric Froude numbers for the upper and lower layers equals to unity, i.e. Eq. 5. A one-dimensional approach is applicable for determining the discharge from two layers. The one-dimensional energy equation is written between a point sufficiently upstream from the sink and control section A, as follows:

$$\frac{1}{2}\rho_1(u_{1a}^2-u_1^2) - \frac{1}{2}\rho_2(u_{2a}^2-u_2^2) = \Delta\rho g(y-h_2) \tag{4}$$

where

$$u_{1a} = \alpha_1 q_1/(h_1+h_2-y),\ u_{2a} = \alpha_2 q_2/y,\ u_1 = q_1/h_1\ ,\ u_2 = q_2/h_2$$

q_i = discharges per unit width from each layer; $i(=1,2)$= subscripts denoting the upper or lower layer; u_i = mean velocities in each layer far upstream;

$u_{1a} = q_1/(h_1+h_2-y)$, $u_{2a} = q_2/y$ = mean velocities in each layer at the control section A; α_i = velocity coefficients (ratio of the velocity at point on the interface to the mean uniform velocity); h_i = layer depths of uniform flow region at the upstream; y = interface position at point A; ρ_i = densities of the fluids; $\Delta\rho(=\rho_2-\rho_1)$= density differences between both fluids of the upper and lower layers.

Differentiating Eq. 4 with respect to y, the following equation at the control section is obtained.

$$\frac{\rho_1 u_{1a}}{\Delta\rho g(h_1+h_2-y)}+\frac{\rho_2 u_{2a}}{\Delta\rho g y}=1 \tag{5}$$

Combining Eqs. 4 and 5, the relationship between withdrawal ratio $r=q_1/q_2$ and the densimetric Froude number $F_r=q_t/\sqrt{\Delta\rho g h_2^3/\rho_1}$ ($q_t=q_1+q_2$: total intake discharge) are derived as follows:

$$r\equiv\frac{q_1}{q_2}=\left\{\frac{\rho_2}{\rho_1}\frac{\alpha_2^2}{\alpha_1^2}\frac{(1+m-m\eta)^3 m(3\eta-2-\eta^3/\alpha_2^2)}{(m\eta)^3[1+3m-3m\eta-(1+m-m\eta)^3/\alpha_1^2]}\right\}^{1/2} \tag{6-1}$$

$$F_r\equiv\frac{q_t}{\sqrt{\Delta\rho g h_2^3/\rho_1}}=\left[\left\{\frac{1}{\alpha_1^2 m^2}(1+m-m\eta)^3(3\eta-2-\eta^3/\alpha_2^2)\right\}^{1/2}+\frac{\rho_1}{\rho_2}\frac{\eta^3}{\alpha_2^2}(1+3m-3m\eta)-(1+m-m\eta)^3/\alpha_1^2\right\}^{1/2}\Big] \Big/ \left\{1+m-(1+m-m\eta)^3/\alpha_1^2-m\eta^3/\alpha_2^2\right\}^{1/2} \tag{6-2}$$

where $\eta=y/h_2$ = nondimensional depth at point A, treated as a dummy variable between Eqs. 6-1 and 6-2, and $m=h_2/h_1$ = depth ratio.

Putting $r=0$ in Eq. 6-1, the critical discharge for selective withdrawal from the lower layer, q_{2c}, is given as follows:

$$F_c\equiv\frac{q_{2c}}{\sqrt{\Delta\rho g h_2^3/\rho_1}}=\left\{\frac{\eta_c^3}{\alpha_2^2}\cdot\frac{1+3m-3m\eta_c-(1+m-m\eta_c)^3/\alpha_2^2}{1+m-m\eta_c^3/\alpha_2^2-(1+m-m\eta_c)^3/\alpha_2^2}\right\}^{1/2} \tag{7}$$

where F_c = critical densimetric Froude number and η_c = a solution for the equation $3\eta_c^2-\eta_c^3/\alpha_2^2=0$. The dummy variable η in Eq. 6 then varies within $\eta_c\leq\eta\leq 1$.

Experimental Results and Discussion

(1) Velocity profiles

Fig. 7 represents the measured velocity profiles at several vertical sections. The height z above the bottom and the horizontal coordinate x are normalized by using the total depth H_t. The horizontal velocity U is

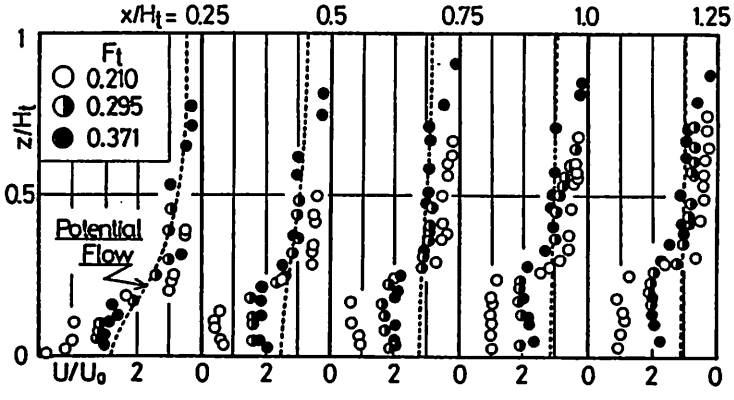

Fig. 7 Normalized distribution profiles of observed horizontal velocity in a two-layer system

non-dimensionalized with respect to the vertical mean velocity $U_0 = q_t/H_t$. The experimental data are varied with the densimetric Froude number, $F_t = q_t/\sqrt{(\Delta\rho/\rho_1)H_t^3}$. To examine the buoyancy effects on the flow fields, solutions of homogeneous potential flow are shown by the broken lines. The observed vertical profiles of velocity in each layer is approximately uniform in the upstream region of $x/H_t \geqq 0.5$. Since the control section is located at a further upstream of $x/H_t \geqq 1.25$, it is justified to apply the one-dimensional flow analysis. As F_t decreases, the velocity difference between the upper and lower layers increases due to the increase of buoyancy at the interface. On the other hand, for large values of F_t, the flow behaves like the potential flow, as if no density effects are present.

(2) Critical condition for incipient drawdown of interface

To verify appropriateness of Eq. 7 representing the critical condition for incipient withdrawal at the upper layer, the tests are executed. For small flow rates there is no withdrawal from the upper layer. As the discharge increases, a stagnant wedge-like region of intermediate-density fluid is formed at the upstream side of the sink. The incipient drawdown of the upper layer takes place just after the wedge disappears. This wedge-like region however tends to obscure the visual indication of incipient withdrawal, and thus we must indirectly estimate the critical condition from the relationship between the withdrawal ratio and the Froude number, as follows.

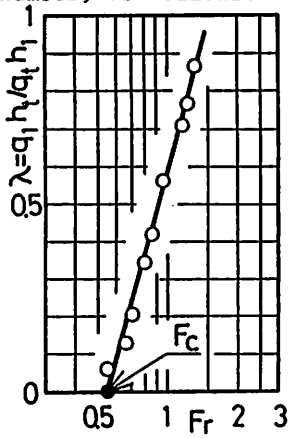

Fig. 8 Determination of critical Froude number F_c for incipient drawdown

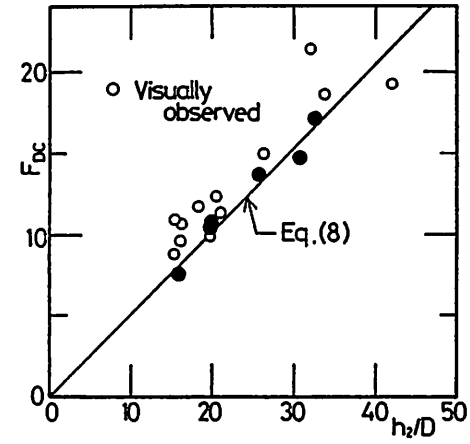

Fig. 9 Relationship between critical densimetric Froude number F_{Dc} and non-dimensional interfacial height above the sink h_2/D

The specific withdrawal ratio is defined as $\lambda \equiv (q_1/q_t)\cdot(H_t/h_1)$, which is a more universal expression than the withdrawal ratio $r = q_1/q_2$ discussed later. Plotting the relationship between λ and the Froude number $F_r = q_t/\sqrt{\Delta\rho g h_2^3/\rho_1}$ as shown in Fig. 8, the critical densimetric Froude number F_c for the incipient withdrawal can be obtained by extrapolating the value of F_r corresponding to $\lambda = 0$.

The results are shown in Fig. 9. In this figure, to examine the effects of the opening height of slot D upon the critical condition, a newly defined critical Froude number, $F_{Dc} = (q_{2c}/D)/\sqrt{\Delta\rho g h_2^3/\rho_1}$, is plotted as a function of h_2/D in the same manner as for the skimmer wall. Visually observed data are shown in the open circles in the figure. By using Fc in Eq. 7, the critical condition can be written as follows:

$$F_{Dc} = F_c \cdot \frac{h_2}{D} \tag{8}$$

Putting $\alpha_2^2 = 1.4$ in Eq. 7, $F_c = 0.51$ is obtained as the best fit value. Since D can be eliminated from both sides of Eq. 8, we conclude that the critical condition for the incipient withdrawal is independent of the opening size of the sink and that intake can be treated as a two-dimensional point sink.

The value of α_2 is considered to be an empirical coefficient including the effects of non-uniformity of velocity distribution, and experimental errors in the

determination of critical conditions. From the fact that α_2 nearly equals unity even in the region near the sink where the non-uniformity of velocity distribution is large, we can again confirm that the one-dimensional analysis is available within the present experimental conditions.

(3) Withdrawal ratio

Beyond the critical intake discharge, fluids in both layers start to move. In this section, the theory for the withdrawal ratio discussed in the foregoing section is verified by our experimental data.

As shown in Fig. 7, the flow asymptotically approaches homogeneous flow with increased densimetric Froude numbers, as if no density effects were present. In the flow fields of sufficiently large F_r, the buoyancy effects become so small that $r=q_1/q_2$ approaches the limiting value $r=h_1/h_2$. Therefore, the specific withdrawal ratio $\lambda=(q_1/q_t)\cdot(H_t/h_1)$ defined in the last section is a more universal and useful parameter than r to express the withdrawal ratio because λ always approaches unity with the increase of F_r, independently of layer depth ratio m. λ relates to r as follows:

$$\lambda = \frac{r}{r+1}(m+1) \tag{9}$$

Fig. 10 shows the experimental and theoretical results of the relationships bewteen λ and F_r. The author's experimental data are plotted in circles and Huber's data (3) in triangles. Curves show the theoretical solutions obtained from Eq. 6.

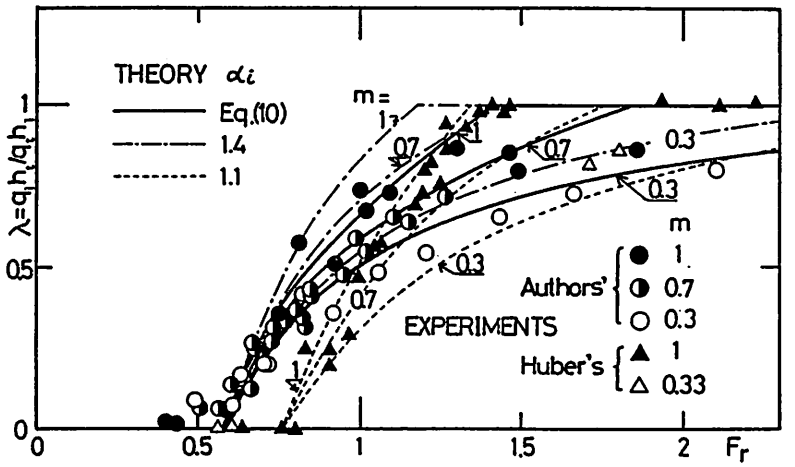

Fig. 10 Specific withdrawal ratio as a function of dimensionless total discharge F_r

Since the magnitude of α_1 and α_2 may significantly affect the theoretical solution of Eq. 6, we must decide the value of α_i in a reasonable way by considering the observed flow characteristics. For small discharges slightly larger than the critical value, $\alpha_i=1.4$, which is obtained from the critical condition (Fig. 9) may be appropriate. In this case, the control section is located near the sink; the fluid flows radially towards the sink at the control section. On the other hand, increasing the flow rate, the position of the control section moves towards the upstream uniform flow region, and thus both α_1 and α_2 may reduce to unity because of the decrease of deformation in the velocity profiles. We see in the figure that the experimental data distribute between the chain and dotted curves theoretically estimated by Eq. 6 with the values of $\alpha_1=\alpha_2=1.4$ and $\alpha_1=\alpha_2=1.1$, respectively. Based on these considerations, we relate the velocity coefficients with the non-dimensional depth of virtual control section, η, as follows:

$$\alpha_1^2 = \alpha_2^2 = (\alpha_c-\alpha_0)\exp.\left[-\beta\frac{\eta-\eta_c}{1-\eta_c}\right] + \alpha_0 \tag{10}$$

where, $\alpha_c=1.4$ and $\alpha_0=1.0$.

Putting $\beta=3.0$ in Eq. 10, the theoretical solutions shown in the solid curves best fit the experiments for any depth ratio m.

Comparison of The Present Analysis with Other Theories and Experiments

Fig. 11 represents the relationship between the square of the ratio of the Froude numbers $r^2=F_1/F_2$ and the sum of two F_1+F_2, where $F_1=q_1/\sqrt{\varepsilon g h_1^3}$, $F_2=q_2/\sqrt{\varepsilon g h_2^3}$ and $\varepsilon=\Delta\rho/\rho_1$. Solid circles denoting the experimental data by Huber and Reid (3) are also plotted.

Jirka's theoretical solution for the skimmer wall (5) (chain line in the figure) gives the values of r^2 considerably larger than the experimental results because his analysis does not consider the approaching velocity head at the far upstream region.

Huber (4) has developed a potential flow analysis in the two-layer system applying a relaxation technique based on an assumption of the interfacial shape and stream function values. It may be seen in the figure that his numerical solution (broken line) is considerably lower than not only our data but his own experimental data (3). This discrepancy may arise from the fact that his analysis were performed under the supercritical flow condition, i.e. $F_1^2+F_2^2 \geq 1$. Such supercritical condition may seldom happen in practical withdrawal system, therefore, application of this theory shall be extremely limited.

On the other hand, our proposed one-dimensional analysis considering the upstream approaching velocity head exhibits good quantitative agreement with his experiment either when the velocity coefficients are fixed (dotted line) or when they are varied with η (solid line).

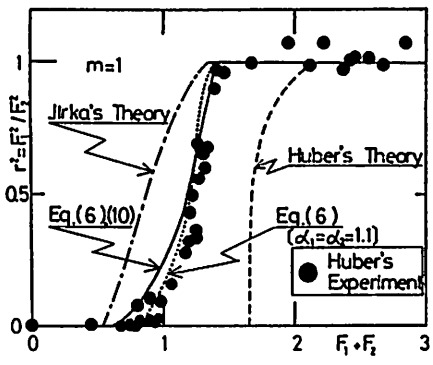

Fig. 11 Comparison of theoretical curves for F_1^2/F_2^2 versus F_1+F_2 with other experimental data and theories

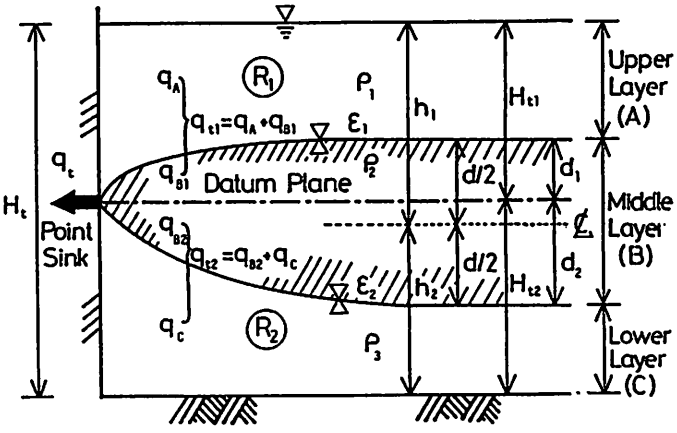

Fig. 12 Schematic of a three-layer system under the study

WITHDRAWAL FROM A THREE-LAYER SYSTEM

Theory

Consider the case of a three-layer system with a point sink at the vertical wall, as in Fig. 12. Let a fictious datum plane be taken at the level same to the sink. Each of the upper and lower two-layer subsystems divided by this plane then becomes geometrically analogous to a two-layer system with a sink at the bottom corner. Extending the theory discussed in the last section to the present system, we develop an analysis to evaluate the outflow discharge from each layer.

If we assume that the fluid in each layer flows parallel to the horizontal plane and has vertically uniform velocity distribution, we can treat the datum plane as one of streamlines in the middle layer. Dividing the middle layer into two regions by this streamline, the ratio of discharges in the two subdivided regions q_{B1}/q_{B2} becomes

$$q_{B1}/q_{B2} = d_1/d_2 \tag{11}$$

where d_1 and d_2 = layer depths divided the middle layer, and q_{B1} and q_{B2} must satisfy

$$q_B = q_{B1} + q_{B2} \tag{12}$$

Next, expressing the functional relationship of Eq. 6 as $r = func.(F_r, m)$ and applying it to the two-layer subsystems above and below the datum plane, respectively, the following equation is obtained:

$$r_j = func.(F_{rj}, m_j) \qquad (j=1,2) \tag{13}$$

where $j\,(=1,2)$= subscripts denoting the quatities in the upper and lower subsystems, respectively; $r_1=q_A/q_B$, $r_2=q_C/q_B$ = discharge ratios for the upper and lower two-layer subsystems; $m_j=d_j/(H_{tj}-d_j)$ = depth ratios; $F_{rj}=q_{tj}/\sqrt{\varepsilon_j g d_j^3}$ = the densimetric Froude number; $\varepsilon_1=(\rho_2-\rho_1)/\rho_1$, $\varepsilon_2=(\rho_3-\rho_2)/\rho_3$ = relative density differences, and q_A, q_B, q_C = discharges per unit width in the upper, middle and lower layers, respectively, which must satisfy the following relationships;

$$\begin{aligned} q_{t_1} &\equiv q_A+q_{B1} = (1+r_1)q_{B1} \\ q_{t_2} &\equiv q_{B2}+q_C = (1+r_2)q_{B2} \end{aligned} \tag{14}$$

where q_{t_1} , q_{t_2} = partial intake discharges for the upper and lower two-layer subsystems, respectively.

Defining the ratio as $\hat{r}=q_{t_1}/q_{t_2}$, the total discharge is written by $\hat{r}$ as

$$q_t = (1+\hat{r})q_{t_2} = (1+\hat{r})/\hat{r}\cdot q_{t_1} \tag{15}$$

Combining Eqs. 11 and 14, the following relationship is derived.

$$\hat{r} = \frac{r_1+1}{r_2+1}\cdot\frac{d_1}{d_2} \tag{16}$$

To obtain the correct withdrawal ratios r_1 and r_2 satisfying all of Eqs. 13, 14 and 15, an iteration technique is used. Computation procedures are as follows:

a) Assume $\hat{r}_0$ as an initial guess of $\hat{r}$ for a given total discharge q_t and compute the partial discharges q_{t1} and q_{t2} from Eq. 15.
b) Calculate r_j corresponding to q_{tj} by using Eq. 13.
c) Substituting r_j into Eq. 16, the value of $\hat{r}$ is then obtained.
d) Check to determine if $\hat{r}=\hat{r}_0$ is satisfied. If not, substitute $\hat{r}$ into $\hat{r}_0$ and iterate the same procedures from (i) to (iv).

Once the computation is accumulated, a set of discharges, q_A, q_B and q_C, can be calculated by using the correct values of $\hat{r}$ and r_j . Fig. 13 shows the flow chart of the above computation procedures.

Experimental Results and Discussion

1) General description of flow fields

Variation in flow pattern with increasing intake discharge are shown schematically in Fig. 14. For small intake discharge, both the upper and lower interfaces are kept horizontal, and only the middle-layer fluid is in motion (Fig. 14(a)). In this stage, two wedge-like stagnant regions with intermediate density appear just upstream of the sink. As the discharge increases, one of the stagnant regions is removed and the first critical condition is achieved (Fig. 14(b)). After the first incipient drawdown (or drawup), two-layer fluids flow towards the intake and only one stagnant region remains (Fig. 14(c)). With further increasing discharge, the second incipient drawdown (or drawup) of another interface occurs just after the disappearance of the last stagnant wedge (Fig. 14(d)). In the final stage, all three layers of fluids flow (Fig. 14(e)).

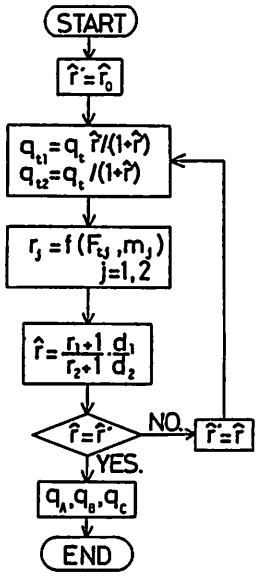

Fig. 13 A flow chart of computation procedures for determination of withdrawal ratio in a three-layer system

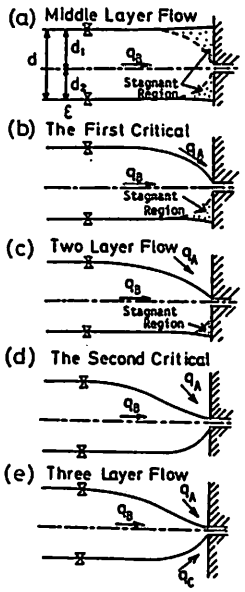

Fig. 14 A variation of flow pattern with increased intake discharge

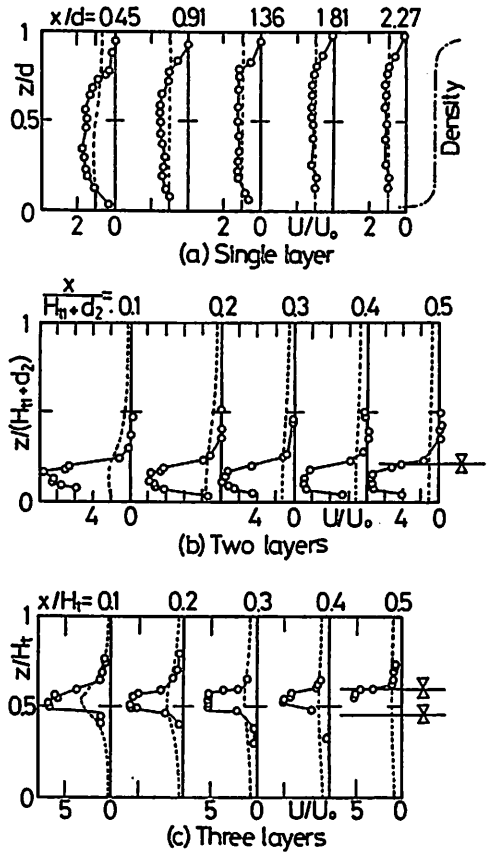

Fig. 15 Normalized distribution profiles of horizontal velocity

The velocity distribution profiles in each stage are shown in Fig. 15, where the horizontal distance from the sink, x , and the vertical location, z are normalized with respect to the depths of the flowing layer in each stage. Horizontal velocity U is presented in dimensionless form by means of average velocity scale U_0 defined from q_t and the depth of the current in each stage. For the purpose of comparison, the analytical solutions for the homogeneous potential flow are shown by dotted curves. The results are summarised as follows:

(a) In the first stage, where only the fluid in the middle layer flows (Fig. 15(a)), the velocities defect in the upper and lower stagnant wedge regions near by the intake. On the other hand, the velocity far upstream has an approximately uniform vertical distribution like that in the potential flow.

(b) When the fluids in the two layers are in motion (Fig. 15(b)), the one velocity defect is observed only in the lower side of the middle layer at the downstream end.

(c) After all layer fluids start to move, there are no velocity defects (Fig. 15(b)).

Throughout all three stages, the uniformity of the velocity in the upstream region where the control section is located is always maintained within each layer. It is confirmed from these results that the one-dimensional energy equation can accurately be applied to the present three layer system, as it is so to the two-layer system.

(2) Experimental verification of the proposed analysis

Fig. 16 shows experimental and analytical results of the relationship between the discharge in each layer and the total intake discharge. The abscissa denotes the dimensionless total discharge, $F_t=q_t/\sqrt{\varepsilon_1 g H_t^3}$ which is a sort of Froude number, normalized by the entire depth H_t as well as relative difference of density ε_1. The

ordinate denotes the normalized discharges from each layer, $(F_A, F_B, F_C)=(q_A, q_B, q_C)/\sqrt{\varepsilon_1 g H_t^3}$. The figure shows quatitatively good agreement between the theoretical curves and the experimental data in every case, which suggests the appropriateness of the present analysis.

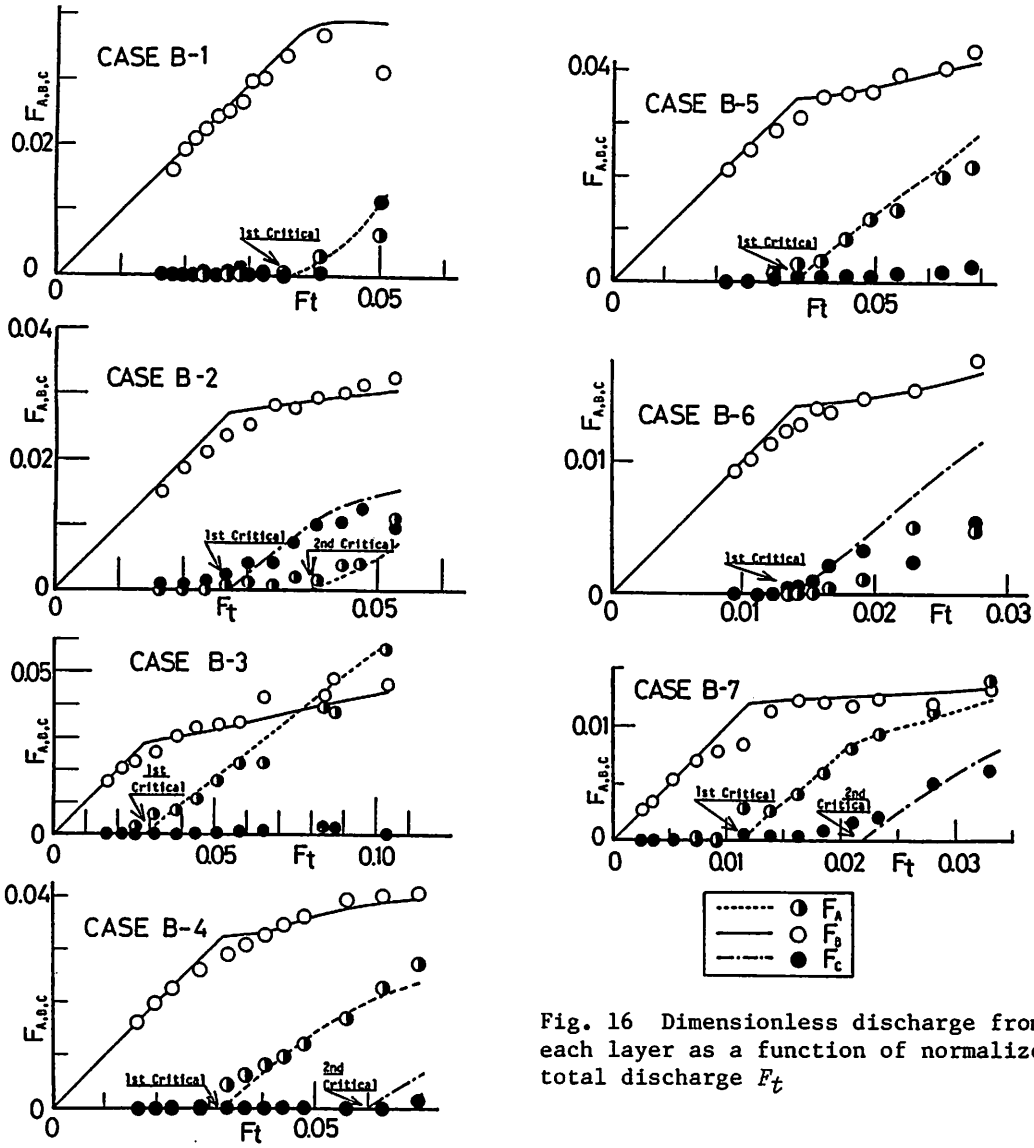

Fig. 16 Dimensionless discharge from each layer as a function of normalized total discharge F_t

APPLICATION TO PRACTICAL PROBLEMS (I) --- EFFECTIVE REMOVAL OF MIDDLE-LAYER FLUID FROM A THREE-LAYER SYSTEM

A three-layer density stratification due to turbidity and temperature complex is often produced after the inflow of fine sediment particles into the thermally stratified reservoir, as shown in Fig. 2. One of the most effective methods of reducing the long retardation of turbid materials in a reservoir is the selective withdrawal of suspended material. In addition, by removing the suspended sediment as soon as possible we can avoid the reduction in the useful life of the reservoir resulting from sedimentation. Although selective withdrawal equipments are installed in most of the recently constructed reservoirs, they have been operated only in rather empirical way to remove turbidity. If the hydraulic behavior of the withdrawal flow fields in such a system is sufficiently understood, the withdrawal equipments can be more efficiently operated.

In this section, we focus our attention on this problem, and propose an optimum intake height for the removal of turbid fluid in the middle layer, based on the above discussed theory.

As examples, we consider nine cases of three-layer systems with various hydraulic conditions, as shown in Table 3. By using the present analysis, we obtain the relationship among the total discharge, the intake height, and the

Table 3 Computational conditions for three-layer systems

h_2/H_1 \ $\varepsilon_1/\varepsilon_2$	0.2	1.0	5.0
0.25	C-1	C-2	C-3
0.50	C-4	C-5	C-6
0.75	C-7	C-8	C-9

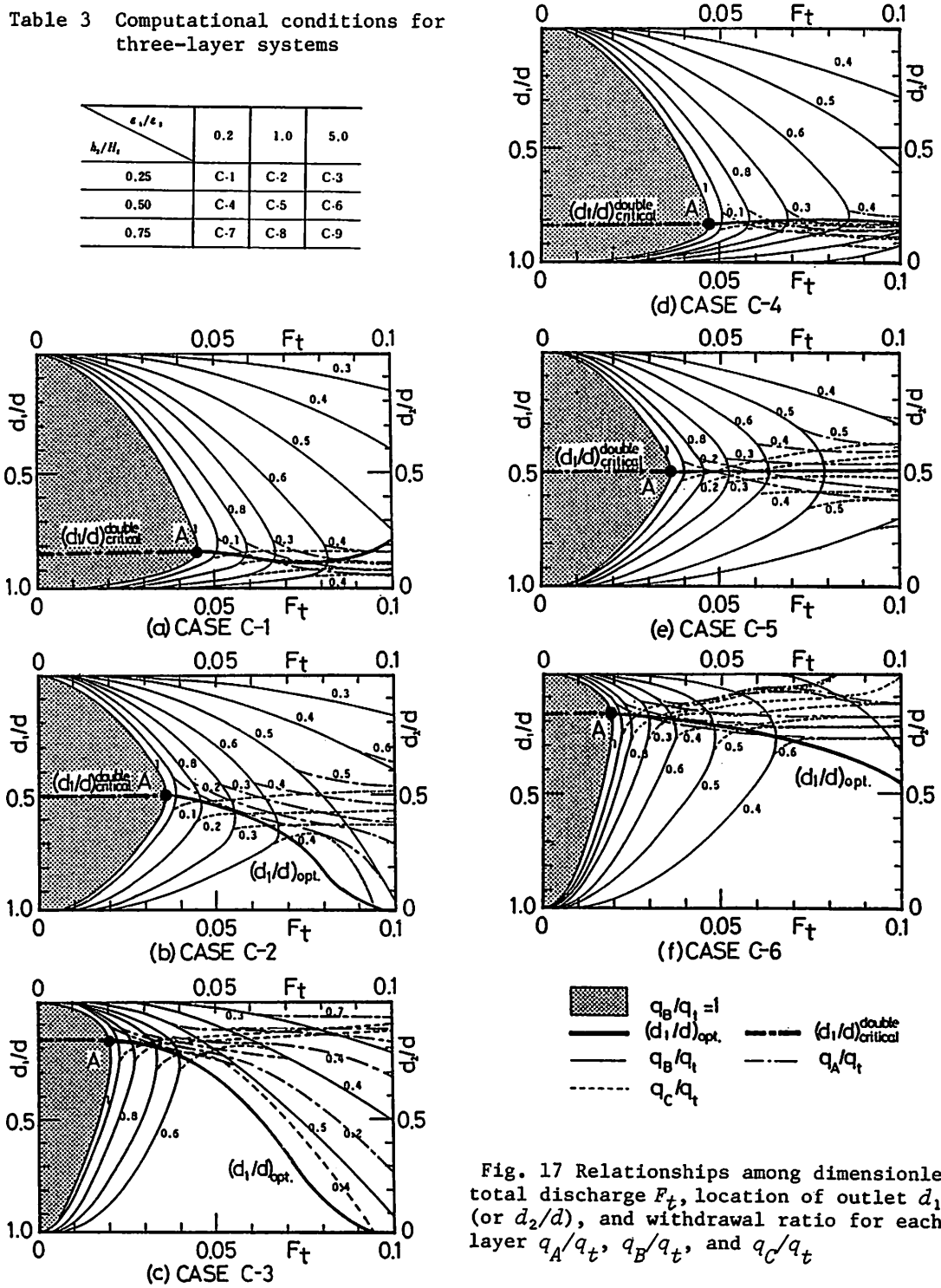

Fig. 17 Relationships among dimensionless total discharge F_t, location of outlet d_1/d (or d_2/d), and withdrawal ratio for each layer q_A/q_t, q_B/q_t, and q_C/q_t

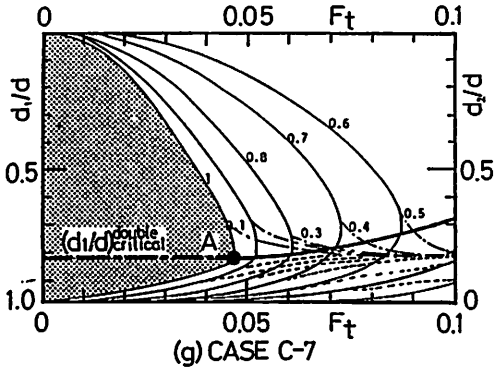

(g) CASE C-7

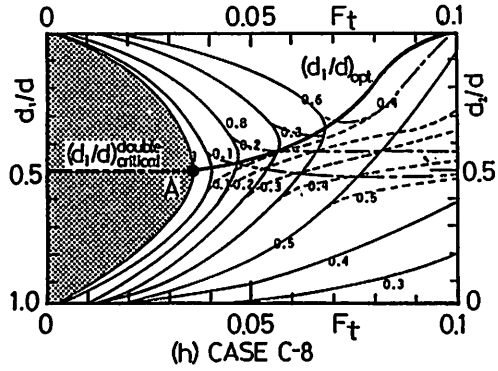

(h) CASE C-8

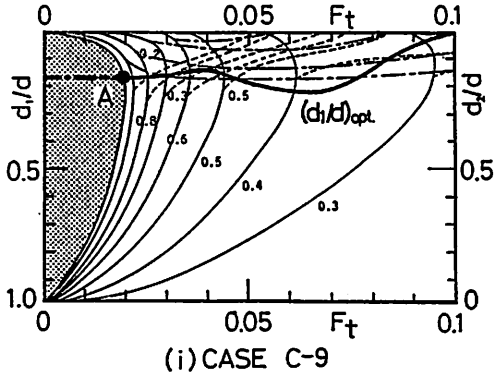

(i) CASE C-9

Fig. 17 Realationships among dimensionless discharge F_t, location of outlet d_1/d (or d_2/d), and withdrawal ratio for each layer q_A/q_t, q_B/q_t, and q_C/q_t

(continued)

outflow discharge from each layer in each case. The calculated results are presented in Fig. 17, where the abscissa denotes F_t and the ordinate, the non-dimensional intake height d_1/d (or d_2/d). The chain, solid, and dotted lines correspond to the equi-value curves of the withdrawal ratios in the upper, middle, and lower layers, q_A/q_t, q_B/q_t and q_C/q_t, respectively. The shaded region represents the area within which only the middle-layer fluid can be removed, i.e. $q_B/q_t=1$. We will call this "the selective withdrawal area for the middle layer". From the critical condition for the incipient withdrawal Eq.7, an analytical expression for this area can be written in the following form:

$$F_{tc}^{B} \equiv \frac{q_{tc}^{B}}{\sqrt{\varepsilon_1 g H_t^5}} = Min.(F_{tc}^{u}, F_{tc}^{l}) \tag{17}$$

where q_{tc}^{B} = critical intake discharge for selectively withdrawing only the middle layer; F_{tc}^{B} = non-dimensional form of q_{tc}^{B}; and $Min.(a,b)$ = smaller value of a and b.

F_{tc}^{u} and F_{tc}^{l} in the above formula are defined by the following equations:

$$\begin{aligned} F_{tc}^{u} &= F_c\left(\frac{d}{H_t}\right)^{3/2}\left(\frac{d_1}{d}\right)^{1/2} \\ F_{tc}^{l} &= F_c\left(\frac{d}{H_t}\right)^{3/2}\left(1-\frac{d_1}{d}\right)^{1/2}\left(\varepsilon_1/\varepsilon_2\right)^{-1/2} \end{aligned} \tag{18}$$

By using Eqs. 17 and 18, the outer edge of the selective withdrawal area for the middle layer can be caluculated as indicated in Fig. 17. In order to remove only the middle-layer fluid as much as possible, the outlet may be placed at the level same to point A where F_{tc}^{B} takes the maximum value. At this point, the incipient drawdown takes place simultaneously at the upper and lower interfaces, and its level, denoted by $(d_1/d)_{\text{critical}}^{\text{double}}$, can be derived by putting $F_{tc}^{u}=F_{tc}^{l}$ in Eq.18 as follows:

$$(d_1/d)_{\text{critical}}^{\text{double}} = 1/(1+\varepsilon_1/\varepsilon_2) \tag{19}$$

This is shown by the thick chain line in Fig. 17.

For large discharge beyond the critical value, the fluids in two or all of the three layers start to flow, and thus the optimum height $(d_1/d)_{opt.}$, which gives the maximum withdrawal ratio of the middle layer, $(q_B/q_t)_{max.}$, varies with increasing F_t. The thick solid curves in Fig. 17 show the functional relationship bewteen $(d_1/d)_{opt.}$ and F_t. From the figures, we can see the effects of the hydraulic conditions of stratified systems upon the optimum outlet level that gives the maximum withdrawal flow rate of middle-layer fluid.

Although the discussion is restricted to the two-dimensional system in this section, the present procedures can be also applied to three-dimensional systems as discussed in the next section. In practical reservoirs we can optimize operation of the selective withdrawal equipments for the removal of turbid water and gain the maximum flow rate of the middle-layer by setting the outlet at the desired level, $(d_1/d)_{opt.}$. In addition, the present theory enables us to evaluate the outflow turbidity from the reservoir.

APPLICATION TO PRACTICAL PROBLEMS (II) --- ANALYSIS ON FLOW FIELDS IN THERMALLY STRATIFIED RESERVOIRS

Extending the above discussed analysis to the three-dimensional thermally stratified reservoirs, in this section, thermal structure in a reservoir affected by the three-dimensional withdrawal flow-fileds is predicted.

As shown in Fig. 1, the stratified fields in reservoirs during spring to summer are often divided into three fairly-well-mixed layers by two distinct thermoclines. In order to analytically describe the thermal structure, one must model two main process, one of which is vertical mixing across the thermocline due to surface-stirring, and the other the advective transport resulting from river flow or pumping as well as power generation. Details of the modeling of the former process may be refered in another paper (6). The discussion herein focuses on the modeling of the latter process.

Since the analysis presented in the foregoing section is restricted to the two-dimensional system, it must be modified so that it can describe flow patterns in three-dimensional systems. Consider now the three-dimensional withdrawal from a two-layer fluid system towards a point sink (see Fig. 18). Let us assume that the flow direction is radially towards the sink, and that the interface is defined by an angle ϕ and a radial distance from the sink s. Just as for the two-dimensional case, the difference of Bernoulli's sums across the density interface may be written as follows:

$$\frac{1}{2}\rho_2\left\{\frac{\alpha_2 Q_2}{s^2\theta(\theta_l+\phi)}\right\}^2-\frac{1}{2}\rho_1\left\{\frac{\alpha_1 Q_1}{s^2\theta(\theta_u+\phi)}\right\}^2=\Delta\rho g(Y-r\sin\phi) \qquad (20)$$

Where θ = angle between the vertical walls; θ_u = angle between the datum plane and the upper wall; θ_l = angle between the datum plane and the lower wall; Y = height of the interface above the datum, and the system is assumed to have spherically symmetrical velocity fields.

Differentiating the above equation with respect to s, we have

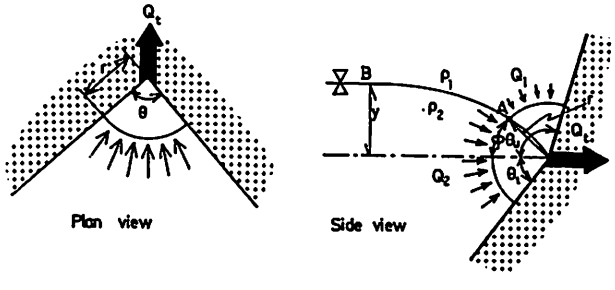

Fig.18 A schematic of simplified flow fields near the sink in a three-dimensional system

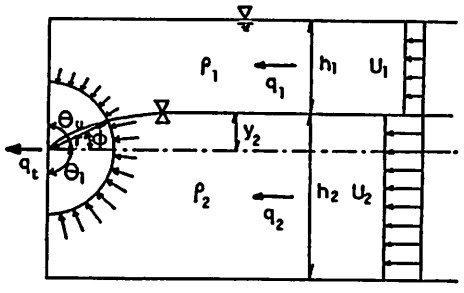

Fig. 19 Axisymmetric assumption in a two-dimensional system

$$(-s\tilde{F}_1^2-s\tilde{F}_2^2+s\cos\phi)\frac{d\phi}{ds}-2(\theta_l+\phi)\tilde{F}_2^2+2(\theta_u-\phi)\tilde{F}_1^2+s\sin\phi = 0 \qquad (21)$$

where

$$\tilde{F}_1^2 = \frac{\rho_1\alpha_1^2Q_1^2}{\Delta\rho g s^5\theta^2(\theta_u-\phi)^3} \quad \text{and} \quad \tilde{F}_2^2 = \frac{\rho_2\alpha_2^2Q_2^2}{\Delta\rho g s^5\theta^2(\theta_l+\phi)^3}$$

are the locally defined Froude numbers.

To satisfy the above equation independently of $d\phi/ds$, we get the following two equations (8):

$$\tilde{F}_1^2-\tilde{F}_2^2-\cos\phi = 0 \qquad (22)$$

$$2(\theta_u-\phi)\tilde{F}_1^2-2(\theta_l+\phi)\tilde{F}_2^2+\sin\phi = 0 \qquad (23)$$

Combining Eqs. 20, 22, and 23, and then simplifying them, the formulae describing the relationship between withdrawal ratio R and total discharge Q_t are derived as:

$$R \equiv \frac{Q_1}{Q_2} = \sqrt{\frac{\rho_2}{\rho_1}}\frac{\alpha_2}{\alpha_1}\sqrt{\frac{(\theta_u-\phi)^3\{(\theta_u+\phi)\cos\phi-1/4\cdot\sin\phi\}}{(\theta_l-\phi)^3\{(\theta_l+\phi)\cos\phi+1/4\cdot\sin\phi\}}} \qquad (24\text{-}1)$$

$$\tilde{F}_r \equiv \frac{Q_1+Q_2}{\sqrt{\Delta\rho g Y^5/\rho_1}} = \frac{Q_t}{\sqrt{\Delta\rho g Y^5/\rho_1}}$$

$$= \left(\frac{4/5}{\sin\phi}\right)^{\frac{5}{2}}\frac{\theta(\theta_u-\phi)^{3/2}}{\alpha_1}\sqrt{\frac{(\theta_l+\phi)\cos\phi-(1/4)\sin\phi}{\theta_l+\theta_u}}$$

$$+\frac{\theta(\theta_l+\phi)^{3/2}}{\alpha_2}\sqrt{\frac{(\theta_u-\phi)\cos\phi+(1/4)\sin\phi}{\theta_l+\theta_u}} \qquad (24\text{-}2)$$

Giving the intake discharge Q_t, the outflow discharges in each layer Q_1 and Q_2 are computed from Eq. 24 in which ϕ is treated as a dummy variable, such as in Eq. 6.

Before we apply the theory to the practical reservoir, we examine appropriateness of the assumption of axisymmetric flow fields in the two-layer model system. Since the analyses on the axisymmetric flow are almost identical to the three-dimensional analyses, except that the later has no lateral spread, we now introduce for convenience a two-dimensional system, as shown in Fig. 19. The details of the analysis for the two-dimensional system are referred in our paper (7), the solution of which has a final form analogous to Eq. 24. The laboratory experiments under the corresponding conditions have been carried out by us, and are

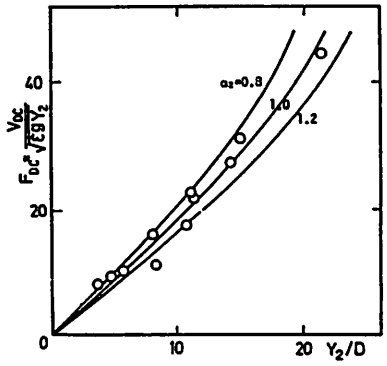

Fig. 20 Critical Froude number F_{Dc} versus non-dimensional interface height above the sink Y_2/D in the two-dimensional system shown in Fig.19

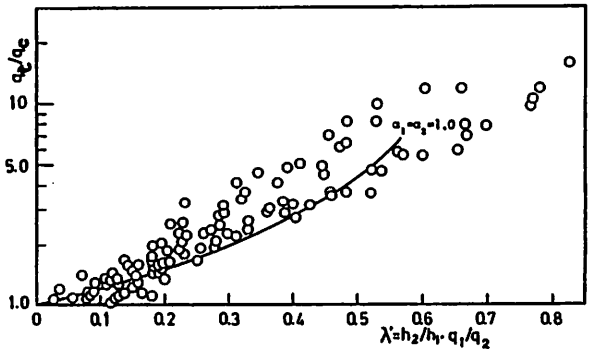

Fig. 21 Total dimensionless discharge q_t/q_c as a function of specific withdrawal ratio $h_2/h_1 \cdot q_1/q_2$ in the two-dimensional system shown in Fig. 19

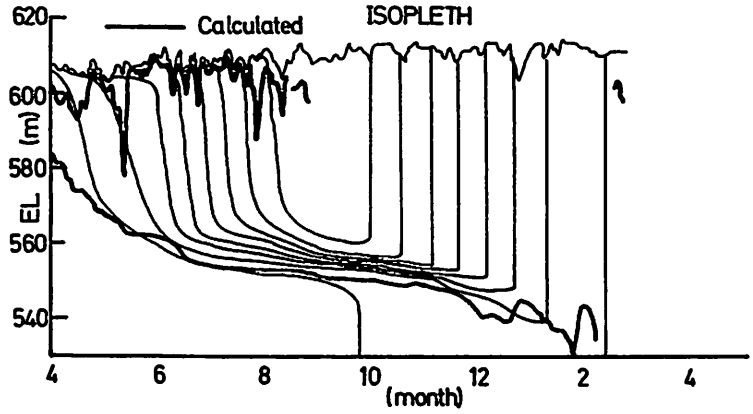

Fig. 22 Comparison between the predicted thermocline location and the observed temperature isopleth in a pumped storage reservoir

compared with the theory as shown in Figs.20 and 21. Fig. 20 shows the results on the critical condition for incipient withdrawal. Fig. 21 shows the relationship between the specific withdrawal ratio and the total discharge. Although the experimental data scatter, a most satisfactory agreement between the theory and experiments is discerned. Therefore, it is concluded that the assumption on the axisymmetric flow field appears to be justified.

Returning to the arguments on the three-dimensional case, our numerical model for the prediction of the thermal structure in a reservoir is summarized as follows.

Substituting Eq. 24 into Eq. 13 and performing the same procedures in the two-dimensional case in Fig. 13, one obtain the solutions for the outflow discharge from each layer in the three-dimensional three-layer system. The inflow properties due to river and pumping discharges are easy to obtain; we assume that the inflow enters the layer at which the density is just greater than or equal to the inflow density. Combining the flow field analysis presented herein with another subroutine on the vertical mixing process, our model is completed. Fig. 22 shows an example of results computed by our proposed model (shown in the thick solid curves) with the observed temperature isopleth. During spring to summer, the advective heat transport process due to inflow and outflow dominates the thermal behavior. On the other hand, the effects of another process, i.e. vertical mixing across the thermocline, are negligibly small. We conclude from the figure that the present analysis is useful for the evaluation of flow patterns not only in laboratory experiments, but in the practical reservoir.

CONCLUDING REMARKS

Intending to analyze the flow fields in the stratified reservoir, a fundamental study of the withdrawal flow in the three-layer system is performed. The analytical results coincide well with our experimental data as well as other researchers'. Applying this theory to the problem of the long retardation of turbidity in stratified reservoirs, we propose a basic idea for the effective removal of turbid middle layer. By operating the selective withdrawal equipments according to our proposed idea, we can not only reduce the long retardation of turbidity but also avoid the reduction of the useful time of a reservoir due to sedimentation. The present analysis is also introduced into our numerical model for the prediction of thermal fields in a reservoir. Although the system is simplified, this model can accurately reproduce the observed thermal structure.

REFERENCES

1. Agemori, C. : Study on water mass behaviors and water quality in man-made reservoir, Technical Report on Research, Grant in Aid for Scientific Research, 1983 (in Japanese).
2. Brooks, N.H. and R.C. Koh : Selective withdrawal from density stratified reservoirs, Journal of Hydraulics Division, Proceedings of ASCE., HY4, pp.1369-1400, 1969.
3. Huber, D.G. and T.L. Reid : Experimental study of two-layered flow through a sink, Journal of Hydraulics Division, Proceedings of ASCE., HY1, pp.31-41, 1966.
4. Huber, D.G. : Irrotational motion of two fluid strata towards a line sink, Journal of Engineering Mechanics Division, Proceedings of ASCE., EM4, pp.71-86, 1960.
5. Jirka, G.H. : Supercritical withdrawal from two-layered fluid systems, Part 1 (Two-dimensional skimmer wall), Journal of Hydraulic Research, Vol.17, pp.43-51, 1979.
6. Murota, A. and K. Michioku : Field observation and numerical modeling of thermal structure in a pumped storage reservoir, Proceedings of 21st Congress of IAHR., pp.335-340, 1985.
7. Michioku, K. and A. Murota : Selective withdrawal from a two-layer stratified system, Proceedings of 33rd Annual Meeting of Japan Society of Civil Engineers, pp.544-545, 1980 (in Japanese).
8. Wood, I.R. : Selective withdrawal from two-layer fluid, Journal of Hydraulic Division, Proceedings of ASCE., HY12, pp.1647-1659, 1978.

APPENDIX - NOTATION

The following symbols are used in this paper:

C_o = observed salinity concentration of the outflow water;

C_B = salinity concentration of the middle-layer fluid;

d = thickness of the middle-layer;

d_1 = vertical distance between the upper density interface and the fictious datum plane;

d_2 = vertical distance bewteen the lower density interface and the fictious datum plane;

$(d_1/d)_{\text{double critical}}$ = value of (d_1/d) to simultaneously occur the incipient drawdown at the upper and lower interfaces;

$(d_1/d)_{\text{opt.}}$ = value of (d_1/d) so as to obtain the maximum discharge from middle layer;

D = opening height of slot;

f_o = observed fluorescence intensity;

f_B = fluorescence intensity of the middle-layer fluid;

$F_i = q_i/\sqrt{\varepsilon g h_i^3}$ = densimetric Froude numbers for the upper and lower layers, respectively, in a two-layer system;

$(F_A, F_B, F_C) \equiv \dfrac{(q_A, q_B, q_C)}{\sqrt{\varepsilon g H_t^3}}$ = non-dimensional discharges per unit width of the Froude type for the upper, middle, and lower layers, respectively;

$F_c \equiv q_{2c}/\sqrt{\Delta\rho g h_2^3/\rho_1}$ = critical densimetric Froude number defined by using h_2;

$F_{Dc} \equiv (q_{2c}/D)/\sqrt{\Delta\rho g h_2^3/\rho_1}$ = critical densimetric number defined by using D;

$F_r \equiv q_t/\sqrt{\Delta\rho g h_2^3/\rho_1}$ = non-dimensional total discharge of the Froude type for a two-layer system;

$F_{rj} \equiv q_{tj}/\sqrt{\varepsilon_j g d_j^3}$ = densimetric Froude number for the upper and lower two-layer subsystems divided by the datum plane;

$F_t \equiv q_t/\sqrt{\varepsilon_1 g H_t^3}$ = non-dimensional total discharge of Froude type for a three-layer system;

$F_{tc}^B \equiv q_{tc}^B/\sqrt{\varepsilon_1 g H_t^3}$ = non-dimensional critical discharge for selectively withdrawing the middle-layer fluid;

$\tilde{F}_1 \equiv \sqrt{\dfrac{\rho_1 \alpha_1^2 Q_1^2}{\Delta\rho g s^5 \theta^2 (\theta_u - \phi)^5}}$ = densimetric Froude number for the upper layer in a three-dimensional two-layer system;

$\tilde{F}_2 \equiv \sqrt{\dfrac{\rho_2 \alpha_2^2 Q_2^2}{\Delta\rho g s^5 \theta^2 (\theta_l + \phi)^5}}$ = densimetric Froude number for the lower layer in a three-dimensional two-layer system;

$\tilde{F}_r \equiv \dfrac{Q_t}{\sqrt{\Delta\rho g y^5/\rho_1}}$ = total discharge of the Froude type in a three-dimensional system;

g = acceleration of gravity;

h_1, h_2 = upper- and lower-layer depths, respectively, in a

two-layer system;

H_t = total depth;

H_{tj} = total depths for the upper and lower subsystems divided by the datum plane in a three layer system;

i (=1,2) = subscript denoting the upper or lower layer;

j (=1,2) = subscript denoting the upper or lower subsystem divided by the datum plane, respectively, in a three layer system;

$m = h_2/h_1$ = layer depth ratio in a two-layer system;

m_j = layer depth ratio in the upper and lower two-layer subsystems in a three-layer system;

q_j = discharges per unit width in the upper and lower layers, respectively, in a two-layer system;

q_A, q_B, q_C = discharges per unit width in the upper, middle, and lower layers, respectively, in a three-layer system;

q_t = total intake discharge per unit width;

q_{2c} = critical intake discharge from the lower layer in a two-layer system;

q_{Bj} = subdivided discharges per unit width in the middle layer corresponding to the upper and lower subsystems, respectively;

q_{tj} = total discharges per unit width for the upper and lower subsystems;

q_{tc}^B = critical total intake discharge per unit width for selectively withdrawing from the middle layer;

Q_1, Q_2 = discharges in the upper and lower layers, respectively, in a three-dimensional two-layer system;

Q_t = total discharge in a three-dimensional system;

$r = q_1/q_2$ = withdrawal ratio in a two-dimensional two-layer system;

r_j = withdrawal ratios for the upper and lower subsystems in a three-layer system;

$\hat{r} = q_{t_1}/q_{t_2}$ = discharge ratios between the total discharges per unit width in the upper and lower subsystems in a three-layer system;

$\hat{r}_0$ = initial guess for $\hat{r}$;

$R = Q_1/Q_2$ = withdrawal ratio for a three-dimensional two-layer system;

s = radial distance from the point sink;

u_i = mean velocities in the upper and lower layers far

upstream in a two-dimensional two-layer system;

u_{ia} = mean velocities in the upper and lower layers at the control section in a two-dimensional two-layer system;

U = observed horizontal velocity;

U_0 = velocity scale defined from q_t and the depth of the current in each stage;

x = horizontal distance from the sink;

y = vertical distance between a point on the interface and the sink;

Y = vertical distance between the interface and the sink far upstream in a three-dimensional system;

z = vertical coordinate;

$\alpha_0, \alpha_c, \beta$ = empirical coefficients in Eq. 10;

α_i = velocity coefficients in the upper and lower layers, respectively;

$\epsilon = \Delta\rho/\rho_1$ = specific density difference across the interface in a two-layer system;

ϵ_j = specific density differences at the upper and lower density interfaces in a three-layer system;

$\eta = y/h_2$ = normalized value for y and treated as a dummy variable in Eq. 6;

θ = angle between the vertical walls;

θ_u = angle between the datum plane and the upper wall;

θ_l = angle between the datum plane and the lower wall;

$\lambda = (q_1/q_t) \cdot (H_t/h_1)$ = specific withdrawal ratio;

ρ_1, ρ_2, ρ_3 = fluid density in each layer;

$\Delta\rho$ = density difference at the interface and

ϕ = angle measured from datum through sink to point on interface.